THE JOURNAL OF PHYSICAL CHEMISTRY C

Article

pubs.acs.org/JPCC

Theoretical Study of Li-Doped sp^2–sp^3 Hybrid Carbon Network for Hydrogen Storage

Yanwei Wen,[†] Xiao Liu,[‡] Xianbao Duan,[†] Kyeongjae Cho,[§] Rong Chen,*[,‡] and Bin Shan*[,†,§]

[†]State Key Laboratory of Materials Processing and Die and Mold Technology and School of Materials Science and Engineering, and [‡]State Key Laboratory of Digital Manufacturing Equipment and Technology and School of Mechanical Science and Engineering, Huazhong University of Science and Technology, Wuhan 430074, Hubei, People's Republic of China

[§]Department of Materials Science and Engineering, The University of Texas at Dallas, Richardson, Texas 75080, United States

Supporting Information

ABSTRACT: Nanoporous carbon structures are promising candidates for hydrogen physisorption storage due to their high specific area and light weight. Using first-principles calculations, we predict a type of sp^2–sp^3 hybrid carbon network (HCN) with well-aligned and size-tunable nanopores that are suitable for hydrogen storage. The unique shape of the nanopores is beneficial for the selective Li atoms doping and induces an enhanced H_2 binding energy that can be attributed to the improved interaction between polarized H_2 and Li ion. A maximum weight percentage of hydrogen storage reaches 6.28 wt % with an average binding energy of −0.19 eV in Li-doped HCN. Together with the ultrahigh volumetric density of hydrogen (102 g/L), the HCN structure is a promising candidate for the hydrogen storage medium.

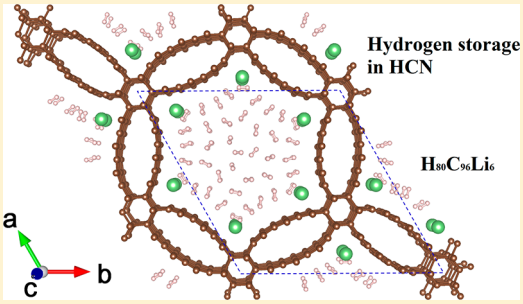

1. INTRODUCTION

Hydrogen is a clean, nontoxic, renewable energy carrier and can be considered as a potential major alternative to fossil fuels for its efficiency, abundance, and environmental friendliness. However, one of the most difficult challenges for the hydrogen economy is the lack of suitable hydrogen storage systems with high gravimetric and volumetric density. The 2015 target of United States Department of Energy (USDOE)[1] requires the medium to carry the hydrogen capacity with 5.5 wt % and 40 g/L volumetric density. In addition, to enable H_2 reversible adsorption/desorption under operating conditions, the adsorption energy in the storage media is desired to be −0.1 to −0.5 eV/H_2. Metal hydrides show high gravimetric and volumetric densities of H_2 storage but suffer from the strong binding energy and poor diffusion rate. Liu et al. find the Li doping into MgH_2 could overcome such drawbacks at low Li doping concentrations.[2] Carbon nanomaterials have attracted a lot of attention for the large surface area and light weight. However, pristine carbon nanostructures are too chemically inert to act as possible hydrogen storage media. These materials such as carbon nanotubes,[3−5] graphite expanded structures,[6−8] and so on suffer from one form of practical difficulty, whereas the H_2 physisorptions in the carbon nanostructures are too weak to store hydrogen at room temperature. One possible approach to improve the H_2 binding energy is to modify these pristine nanostructures by doping metal atoms. A lot of studies suggest that the transition metals doping could enhance the H_2 binding energy in carbon nanotubes,[9−12] graphene,[13−15] and graphyne.[16,17] The enhanced binding by transition metal is known as the Kubas bonding,[18] where stems from the hybridization of the σ or σ^* orbitals of the H−H bond with the transition metal d orbitals. Psofogiannakis and co-workers measure a reversible H_2 storage capacity of about 3 wt % in graphite oxide-like carbon foam doped with Pd/Hg nanoparticles at room temperature and 2 MPa pressure.[19] However, the transition metals are prone to form clusters, and it is fundamentally difficult to achieve homogeneous monolayer coating on the carbon nanostructures.[20,21] Furthermore, the Kubas interaction seems to be excessively strong to dissociate the hydrogen molecule, which reduces the amount of the hydrogen storage. Recently, graphene structures doped with light metals such as Li, Ca, and Al atoms have been predicted to store the hydrogen capacity more than 8.4 wt % theoretically.[22−25] Unfortunately, the latest study shows that the hydrogen storage capacity in Al-doped graphene is significantly reduced due to the dissociation of the first adsorbed H_2 molecule.[26] Although it is verified that the Li doping could enhance the hydrogen binding energy in carbon nanotubes and boosts the reversible hydrogen storage to 3.9 wt % at 77 K and 106 kPa,[27] no experiment has yielded comparable hydrogen capacity to the theoretical expectations for the low-dimensional carbon material.

Sigal et al. cast serious doubt about the straightforward application of metal-doped two-dimensional (2D) systems for hydrogen storage since even slight oxygen content in H_2 atmosphere can block the metal sites at ambient condition which suppresses the H_2 adsorption and suppose metal-

Received: March 9, 2015
Revised: June 4, 2015
Published: June 16, 2015

DOI: 10.1021/acs.jpcc.5b02312
J. Phys. Chem. C 2015, 119, 15831−15838

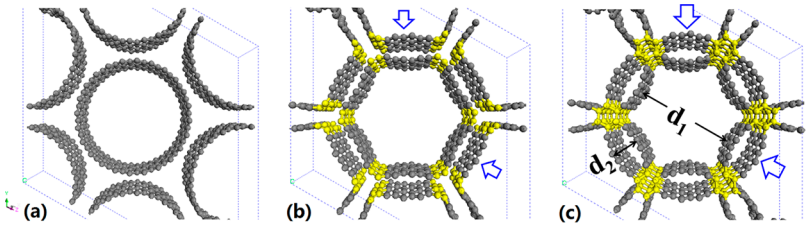

Figure 1. Intermediate configurations of (24, 0) SWCNT bundles upon compressing strain: (a) ideal bundle, (b) hexagonal-like bundle, and (c) HCN structure.

decorated porous structures could be more practical by hindering the oxygen access to the metal sites.[28] In fact, metal-contained three-dimensional nanoporous carbon has been fabricated and exhibits promising application in hydrogen storage.[29] Gogotsi et al. fabricate a series of porous carbide-derived carbons and find the hydrogen storage in TiC-carbide-derived carbon reaches 3.0 wt % at 1 atm pressure and 77 K.[30] Their results indicate that hydrogen storage is dominated by the porous size rather than the total specific surface area. Another work reveals that the density of the adsorbed fluid hydrogen appears to be a function of both the pore size and pressure in carbon nanopores.[31] Recently, metal organic framework (MOF) and covalent organic framework (COF) are proposed to be promising candidates for hydrogen storage due to the chemically tunable nanoporous structures.[32−37] Pt-decorated MOFs are reported to achieve ∼4% mass fraction excess hydrogen storage at 10 MPa gas pressure and room temperature experimentally.[38] Among a series of alkali-metalized MOFs and COFs, MOF200-Li and MOF200-Na are predicted to meet the 2015 USDOE target in weight percentage at 298 K; nevertheless, the highest volumetric density among them is less than 25 g/L.[39] Most recently, a new COF configuration (COF-301) is designed with nanoporous size of about 9 Å, and the grand canonical Monte Carlo simulations suggest PdCl decorated COF-301 exhibits H_2 volumetric density of 60 g/L at 100 bar and room temperature, close to the ultimate target of 70 g/L. However, the H_2 weight percentage in COF301-PbCl is 4.2 wt %, still lower than the goals of 2015.[40] Up to now, none of three-dimensional (3D) nanoporous structures could meet the requirement of hydrogen storage in both weight percentage and volumetric density.

In this work, we reveal that a new type of 3D carbon hybrid carbon network (HCN) with size-tunable and well-aligned nanopores, which can be formed from single-wall carbon nanotubes (SWCNTs) bundles by applying radial pressure. By changing the diameters of SWCNTs, the nanoporous size of HCN can be flexibly tunable, which makes it a promising container for hydrogen uptake. We present that the doping of alkali metal Li to the corner site of the nanopore is selectively favorable, and the unique shape of nanopore prevents the migration and clustering of Li atoms. It is indicated that the H_2 binding energy can be effectively enhanced via polarization of the H_2 in a local electric field caused by Li ions. The maximum weight percentage of hydrogen storage in the HCN achieves to 6.28 wt %, and the corresponding volumetric density is as high as 102 g/L, which reaches the 2015 goals of USDOE. These findings imply the HCN structure could be a promising material in highly efficient H_2 storage.

2. COMPUTATIONAL METHOD

Our density-functional calculations have been performed using the projector-augmented-wave (PAW)[41] method, implemented in the Vienna *ab initio* Simulation Package (VASP).[42−44] It is reported the general gradient approximation (GGA) usually produced purely repulsive interactions between H_2 and graphene as well as carbon nanotube,[45] which contradicts the experimental findings.[46] While local density approximation (LDA) often overestimates the binding energies between H_2 and metal atom as well as carbon planar structure.[47] However, the overestimate of the binding energy by LDA could be compensated by the neglect of the van der Waals (vdW) interactions of H_2 in carbon nanoporous structures,[48] and the H_2 adsorption energies predicted by LDA calculations are in substantial agreement with the second-order Møller−Plesset (MP2) perturbation theory as well as the experiments.[49−51] Moreover, we calculate the H_2 binding energy in the nanopores of Li-doped HCN by several vdW correction methods[52,53] (Table S1 in Supplementing Information) and find the prediction given by LDA agrees well with the corrected results. Thus, LDA is chosen to calculate the binding energy between the H_2 and HCN as well as Li-doped HCN rather than GGA in this work. We adopt a standard hexagonal supercell for the SWCNTs bundle and HCN structures. The plane-wave cutoff is set to 400 eV, and the Brillouin zone of the supercell is sampled with Γ centered Monkhorst−Pack grid of 2 × 2 × 12. The atomic positions are fully optimized until the magnitude of the forces acting on all atoms becomes less than 0.05 eV/Å.

3. RESULTS AND DISCUSSION

As demonstrated in previous studies, ultrasmall diameter zigzag SWCNTs (5, 0) could spontaneously join with each other with covalent bonds rather than weak vdW force due to the intensive curvature[54] and then spontaneously form a hybrid carbon network with size-tunable nanopores.[55] Interestingly, previous work showed that hydrostatic pressure on the SWCNT could make the SWCNT undergo oval and peanut shape transitions with anisotropic curvature.[56] The following observation of the pressure-induced transition in magnetoresistance in SWCNT bundles confirmed an anisotropic shape transition of the SWCNTs upon pressure.[57] Here we present an experimentally accessible approach to achieve the HCN structures for larger diameter SWCNTs bundles by applying radial pressure. We take the (24, 0) SWCNTs bundles for example to investigate the formation of HCN structures. As known, the pristine SWCNTs of (24, 0) are prone to align in a 2D hexagonal lattice to form bundle state as Figure 1a. The equilibrium lattice constants of (24, 0) SWCNTs bundle are calculated to be $a = b = 21.66$ Å and $c = 4.21$ Å, respectively. The optimized individual SWCNT in the bundles appears natural cylinder shape and the distance between neighboring nanotubes is 3.2 Å, which indicates the vdW force is responsible for the stability of the bundle. However, upon radial compressing strain (∼1.9 Å, 9 GPa), the individual nanotubes are enforced to approach to each other and thus exhibit a hexagonal

DOI: 10.1021/acs.jpcc.5b02312
J. Phys. Chem. C 2015, 119, 15831−15838

deformation according to the symmetry of the aligned nanotubes (Figure 1b). If further compressing is applied (~2.6 Å, 12 GPa), we find the sidewalls of hexagonal-like nanotubes become incurved and the vertexes of the hexagonal nanotubes get close to the neighboring ones and eventually covalently bond with each other to form a HCN structure in Figure 1c. It is noticed that the carbon atoms undergone sp^3 hybridization in HCN are marked as yellow, which offer a junction to support the whole structure. The formed HCN structure is in hexagonal symmetry with a shorter lattice constant of $a = b = 18.77$ Å. During the phase transition from the SWCNT bundle to HCN structure, the size of the inner space marked as d_1 in the nanotubes has been compressed from 1.85 to 1.49 nm in Figure 1c. On the other hand, the sidewalls between two neighboring junctions form an oval nanotube with the distance d_2 of 3.8 Å. According to the compressing pressure of ~12 GPa, we estimate an energy barrier of 0.16 eV/C should be overcome during the transformation from regular bundles to HCN structure. It is noticed that such bundle to HCN transformation can be applied for other zigzag SWCNTs. The derived HCN structures exhibit different nanoporous sizes, which correlates to the diameters of the precursor nanotubes. Table 1 summarizes the structural parameters of HCNs derived from different SWCNTs and the sizes of the main nanopores (d_1) of the HCNs range from 9.9 to 20.1 Å. Moreover, we show that HCNs remain quite stable under ambient temperatures once formed and the (24, 0) HCN only transforms reversibly to SWCNT bundles at a temperature of about 1580 K by molecular dynamics simulations (see Figures S1 in Supporting Information).

Table 1. Calculated Structural Parameters of Different HCNs

HCN	(15, 0)	(18, 0)	(21, 0)	(24, 0)	(27, 0)	(36, 0)
a (Å)	12.84	14.76	16.50	18.77	20.71	26.5
c (Å)	4.21	4.21	4.21	4.21	4.21	4.21
d_1 (Å)	9.87	11.58	12.74	14.95	16.33	20.80
d_2 (Å)	2.97	3.18	3.76	3.81	4.38	5.76

Figure 2a shows the calculated electronic band structure and density of state (DOS) of the (24, 0) SWCNT bundle, hexagonally deformed SWCNT bundle, and HCN structure. As indicated by Figure 2a, the band structure of ideal bundle in the Γ−A direction is similar to that of SWCNT, while the bands in-plane appear flatter dispersion than those along the tube axis near the Fermi level, which corresponds to the vdW interaction between neighboring SWCNTs. Thus, the DOS of the ideal bundle show a significant peak at the Fermi level. Upon radial pressure, the individual SWCNTs in the bundle undergo hexagonal deformations and lead to increased area of faced sidewalls of SWCNTs. As a result, the deformed SWCNTs exhibit relatively stronger vdW interaction and thus show enhanced dispersion of the band structure near the Fermi level in Figure 2b. However, once the HCN structure is formed, an obvious band gap of 0.36 eV is opened due to the formation of strong sp^3 C−C bonds in the junction region. The band structure of the HCN exhibits similarly anisotropic features in different directions. The flat bands in the Γ-M-K-Γ directions indicate there is weak dispersion in-plane due to the formation of sp^3 carbon atoms junction, which divides the conducting blocks of sp^2 carbon atoms. It implies that the mass of the carrier moving against the porous axis is much heavier than that along the porous axis near the Fermi level. Along the porous axis, the dispersion of the bands is similar to that of pristine SWCNT except for the opened band gap.

Because of the nanoporous structure and large specific surface area, it is expected that the HCN structure would be much advantageous in hydrogen storage. The physisorption of hydrogen molecules in (24, 0) HCN is investigated first. We notice the HCN structure shows two sizes of nanopores: d_1 and d_2 marked in Figure 1. Since d_2 is much smaller (3.8 Å) than d_1 and the former is too narrow to encapsulate the hydrogen molecules, we focus on the discussion of hydrogen physisorption in larger nanopore d_1. The H_2 attachment to several possible sites in this nanopore has been considered, and we find the stable H_2 physisorption energies for the side and corner sites (Figure 3a) are calculated to be −0.08 and −0.12 eV, respectively. It is noticed the binding energy of the latter is more favorable, which can be attributed to the overlapped attraction of the two adjacent sidewalls. The distances between H_2 and the sidewall of nanopore for the two sites are optimized to be about 2.70 Å, and the H−H bond length in adsorbed H_2 is 0.77 Å. Together with the small negative binding energy, we conclude that there is weak attractive interaction between H_2 and the (24, 0) HCN.

Since the physisorption of H_2 into the pristine nanopore is too weak to store hydrogen at ambient conditions, light metal atom Li is introduced into the nanopore to improve the H_2 binding energy. To evaluate whether the metal atoms cluster or not in the nanopores, the Li binding energies into different doping sites are defined as

$$E_b = E_{Li@HCN} - E_{HCN} - E_{Li\_bcc}$$

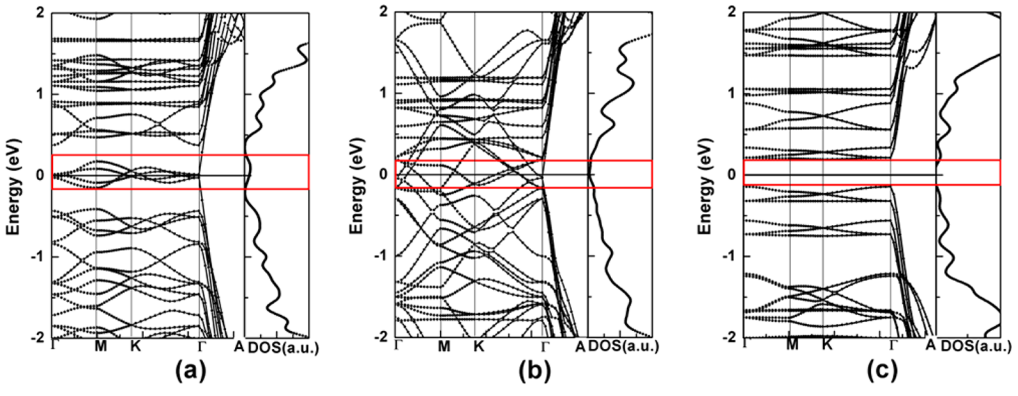

Figure 2. Electronic band structure and DOS of (24, 0): (a) ideal SWCNTs bundle, (b) hexagonal-like bundle, and (c) HCN structure.

DOI: 10.1021/acs.jpcc.5b02312
J. Phys. Chem. C 2015, 119, 15831−15838

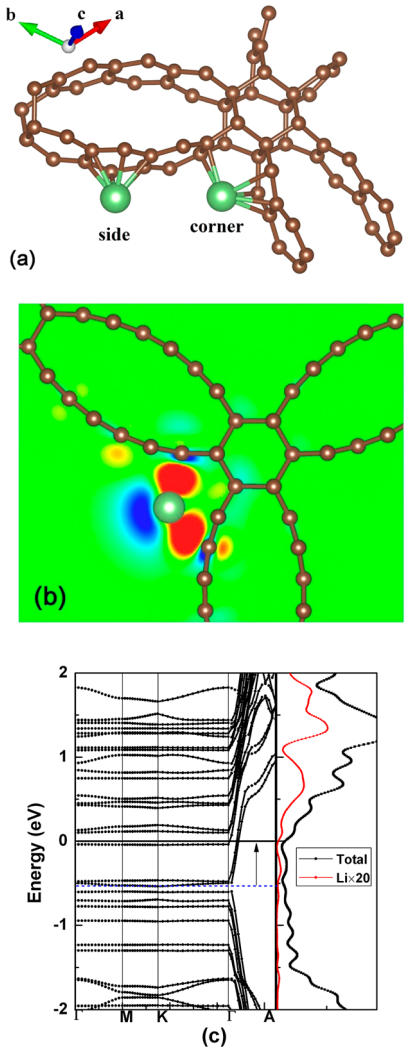

Figure 3. (a) Possible Li doping sites in the nanopores of HCN. (b, c) Differential charge density contour and the band structures as well as the DOS of Li atom doped into the corner site of HCN, respectively.

where $E_{Li@HCN}$ and E_{HCN} denote the total energy of metal atom doped HCN and pristine HCN structure, respectively, and E_{Li_bcc} is the total energy of single Li atom in bcc structure. Thus, a negative binding energy means an exothermic process of the Li intercalation into the HCN. After relaxation, two stable sites have been found for Li doping: the corner site and side site in Figure 3a. It is found that the binding energy of Li doping to corner site is −0.29 eV compared to the bulk Li, which indicates that Li prefers doping rather than clustering in the nanopore. On the other hand, the side site with a flatter curvature exhibits a much higher binding energy of +0.22 eV, which implies the Li would dominantly reside the corner site rather than side site. Figure 3b plots the charge transfer contours between Li and HCN, and there are clear charge loss near the Li atom and charge accumulation near the carbon atoms, which suggests the 2s electron of Li has been transferred to HCN. Our Bader charge analysis[58,59] shows that there are 0.867 e^- of Li donating to HCN and the bond between Li and HCN is ionic-like, which would be responsible for the strong binding energy. As a result, a Li positive ion is exposed in the nanopores upon doping. The charge transfer from Li to HCN agrees well with the change of band structure in Figure 3c, which follows a rigid band picture except for the upshifting of Fermi level upon doping.

The H_2 binding energy to the Li doped into the corner site of HCN (Li@HCN) is defined as

$$E_b = E_{H_2\_Li@HCN} - E_{H_2} - E_{Li@HCN}$$

where the $E_{H_2Li@HCN}$, E_{H_2}, and $E_{Li@HCN}$ are the total energies of H_2 adsorbed Li@HCN, H_2 molecule, and Li@HCN systems, respectively. The optimized configuration of one H_2 adsorbed Li@HCN is shown in Figure 4a. It is found the H_2 molecule is

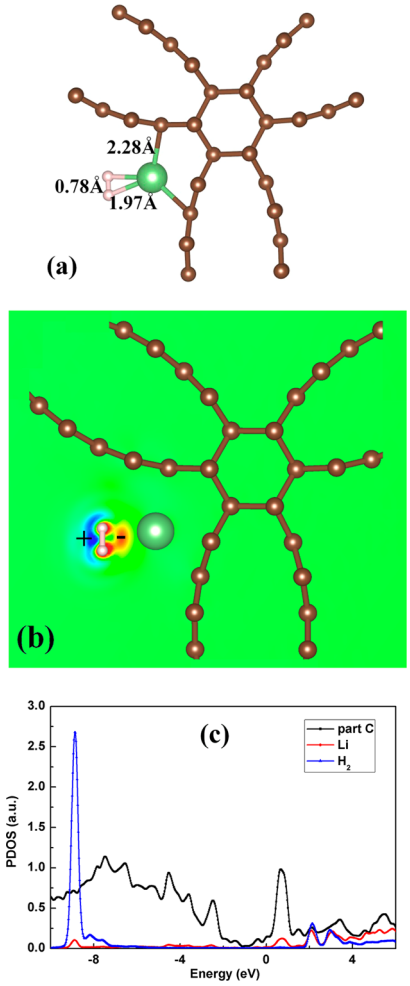

Figure 4. (a) Configuration of H_2 adsorbed onto the Li@HCN with the corner site. (b) Differential charge density of H_2 adsorbed to Li@HCN with polarization. (c) Partial DOS of Li and H atoms as well as the neighboring C atoms in H_2 adsorbed Li@HCN.

parallel instead of heading to the Li ion, and the distance between H_2 and Li ion is 1.97 Å, which is shorter than the vdW adsorption distance (2.70 Å). The binding energy of a H_2 adsorbed to the Li@HCN is −0.28 eV, much stronger than weak physisorption in the bare nanopores. The interaction between Li and H_2 enlarges the bond length of H−H to 0.78 Å. We note the distance between Li and H_2 as well as the H−H bond length in Li@HCN is quite different from that of transition metal atoms doped carbon structures.[60] It is reported that the typical distance between the adsorbed H_2 and Ti is about 1.73 Å, and the H_2 is dissociated with a bond length of 2.71 Å in Ti-doped carbon nanotubes.[11] To throw light on the interaction between H_2 and doped Li ion, Figure 4b shows the differential charge density contour of the H_2 adsorbed Li@HCN across the plane of the one Li and two H atoms, which is defined as $\Delta\rho = \rho(H_2\_Li@HCN)$

DOI: 10.1021/acs.jpcc.5b02312
J. Phys. Chem. C 2015, 119, 15831−15838

$-\rho(\text{Li@HCN}) - \rho(H_2)$. The red and blue colors represent electron accumulation and depletion, and there is obvious charge redistribution of H_2 inside the nanopores of HCN in Figure 4b. The negative charge of H_2 gathers toward the Li ion, and the positive charge departs form Li ion, which indicates the H_2 has been polarized clearly. Moreover, we examine the partial DOS of H_2 adsorbed Li@HCN (Figure 4c) and find the σ orbital of the H_2 located far below the Fermi level remains intact without hybridization with 2s or 2p orbitals of Li, which implies no chemical bonds formed between H and Li. The Bader charge analysis reveals there is no electron of the H_2 transferred to Li, supporting no chemical bonds formed between them. This also agrees with the intact DOS of H_2 in Figure 4c. On the other hand, the charge analysis of Li indicates only 0.847 e^- transfers from Li to HCN upon H_2 adsorption. This is reasonable since the polarization of H_2 (Figure 4b) where negative charge heading to the Li screens the binding between Li and HCN and cause less charge transfer of Li to the HCN. The strong binding between H_2 and Li@HCN should be attributed to the induced electric field by positive Li ion in the nanopores, which is similar to the case of Ca decorated fullerenes.[22] Our calculated H_2 binding energy in Li@HCN is a little stronger than those reported on SWCNTs,[51] which can be attributed to the more charge transfer of Li to the HCN for the unique corner site.

By adding more H_2 molecules to the Li atom, the binding energies for two, three, and four H_2 adsorbed to Li@HCN are calculated to be −0.22, −0.21, and −0.21 eV per H_2, respectively. We note a single Li atom can adsorb up to four H_2 molecules (Figure 5a) with a relatively constant binding energy in the nanopores of HCN, which indicates multiple H_2 adsorption would not weaken the attraction between H_2 and Li. Since there are six equivalent corner sites in each nanopore, it is expected that large amount of H_2 could be stored in the Li@HCN structure. To evaluate the H_2 storage capacity, we increase H_2 concentration gradually into the nanopores and calculate the corresponding total and average binding energies. For each concentration, several configurations of H_2 arrangement inside the nanopores are considered, and the lowest binding energies are plot as a function of the H_2 concentrations in Figure 5b. We notice the total binding energies lower down as the H_2 concentrations increase to $H_{80}C_{96}Li_6$ and further uptake will lead to the increase of the binding energy due to the strong repulsion between H_2 and HCN as well as H_2 and H_2. Thus, the highest H_2 storage capacity in Li@HCN is estimated to be 6.28 wt %. The configuration for $H_{80}C_{96}Li_6$ is shown in Figures 5c and 5d in top and side views, and it is found that the H_2 molecules are arranged in two alternative layers along the nanoporous axis. On the other hand, the average binding energy of H_2 for $H_{80}C_{96}Li_6$ is calculated to be −0.19 eV/H_2. The zero point energies to H_2 molecule in free and adsorbed states have been considered and we find the correction is slight since most of the H_2 in the nanopores are in physisorption states. The binding energy is close to the optimum enthalpy (−0.16 eV/H_2) for H_2 storage upon reasonable pressures at room temperature,[61] which implies the Li@HCN could be favorable for hydrogen reversible adsorption/desorption under mild conditions. Moreover, the H_2 molecules are packed in a high density state in the nanopores and the H_2 volumetric weight percentage is calculated to be 102 g/L in Li@HCN, much higher than the ultimate goals of DOE (70 g/L). The high weight percentage and volumetric density of H_2 uptake indicate the Li-modified HCN should be promising materials for hydrogen storage. Besides that, it is found that the HCN keeps robust structure and the volumetric change of HCN can be negligible with the maximum H_2 uptake.

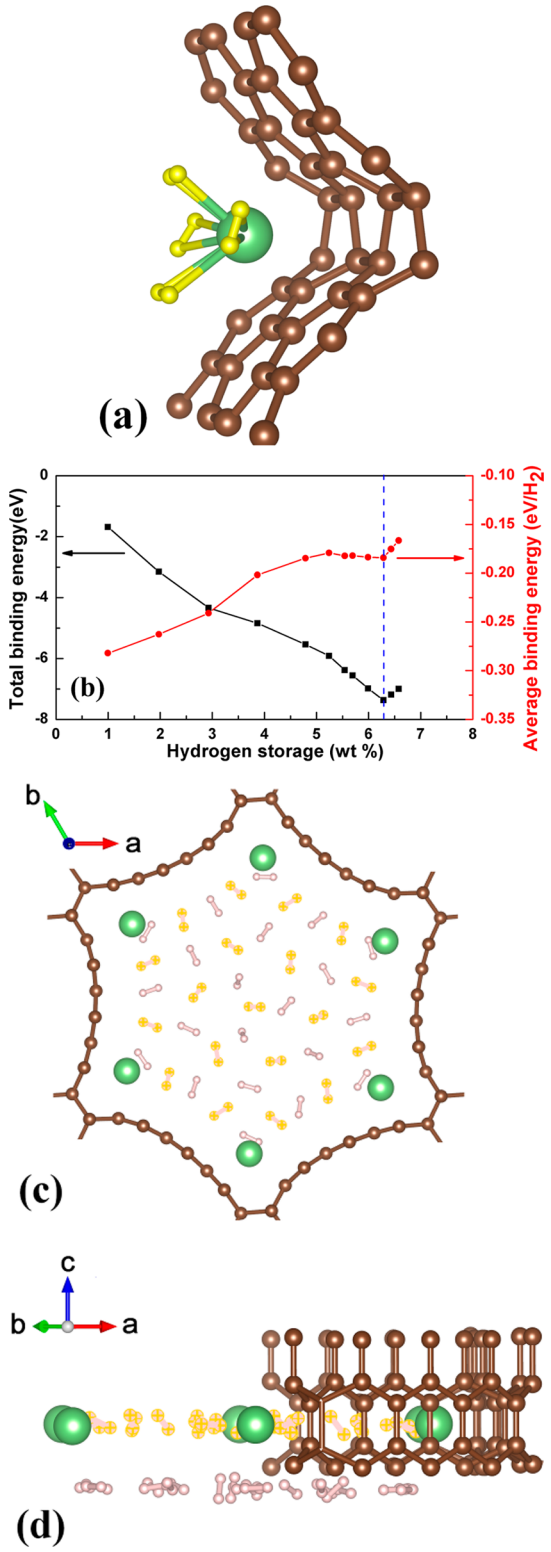

Figure 5. (a) The configuration of four H_2 adsorbed on Li@HCN, (b) total and average binding energies curve to the H_2 adsorption concentration in the nanopores of Li@HCN, (c) and (d) are the top- and side-views of the configurations of maximum H_2 storage in Li@HCN with a formula of $H_{80}C_{96}Li_6$.

To explore the interaction between multiply H_2 molecules and the Li@HCN, the electrostatic potential profiles inside the

DOI: 10.1021/acs.jpcc.5b02312
J. Phys. Chem. C 2015, 119, 15831−15838

nanopores are provided in Figure 6a. The upper inset shows the electrostatic potential contour in the cross section which crosses

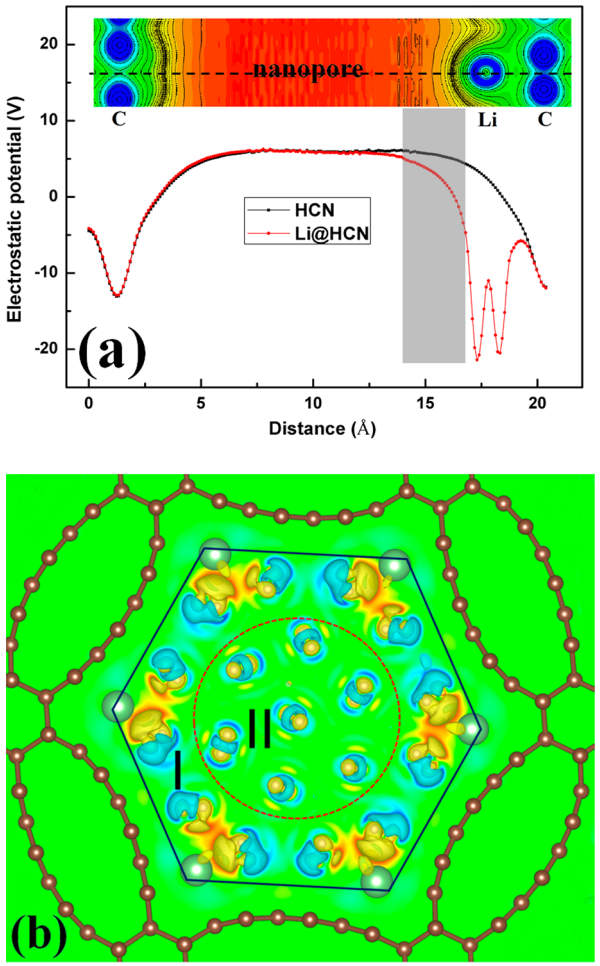

Figure 6. (a) Electrostatic potential plots across the nanopore of HCN and Li@HCN. (b) Differential charge density isosurface of upper layer of the H_2 adsorption indicates the two regions adsorption mechanism of H_2 storage in Li@HCN by different polarized degrees.

the two opposite corner sites of Li@HCN along the nanoporous axis. Figure 6a shows the corresponding potential curves along the line crossing the Li atom norm to nanoporous axis (inset in Figure 6a) for both pristine and Li-doped HCN. The slope of the curve indicates the electric field in the nanopores. At the optimum hydrogen distance, it is found the electronic field intensity of Li@HCN in the gray region ranges $(2-6) \times 10^{10}$ V/m, which is about 4 times that of pristine HCN. Such electronic field is high enough to polarize the H_2 molecules,[62] and thus the enhanced electronic field is responsible for the improved binding between H_2 and Li ion. We note the H_2 molecules keep robust binding (−0.20 eV/H_2) to the Li@HCN until the concentration approaches to $H_{48}C_{96}Li_6$ (3.87 wt %), which corresponds to the formula of $H_{48}C_{96}Li_6$. The configuration of $H_{48}C_{96}Li_6$ is shown in Figure S2, where all the H_2 molecules are directly attached to Li with four H_2 per Li. If more H_2 molecules are introduced, they would be adsorbed as an indirect layer (region II in Figure 6b) in the nanoporous with an average energy gain of −0.16 eV/H_2, which is still strong enough for the H_2 storage. We note the indirect layer H_2's are more than 4 Å away from the Li, and the average binding energy of −0.16 eV should involves two parts: the binding energy between the first layer adsorbed Li@HCN and 16 H_2 cluster, as well as the binding energy between H_2 molecules in the H_2 cluster. The calculated results show the contributions of the two parts to the energy gain are −0.09 and −0.07 eV/H_2, respectively. Moreover, the binding energy between the indirect layer H_2 and the first layer adsorbed HCN ($C_{96}H_{48}$) without Li is calculated to be −0.12 eV/H_2, a little weaker than that of Li@HCN (−0.16 eV/H_2). Thus, the enhanced binding of the indirect layer H_2 should also be attributed to the polarized effect of Li doping. However, the improved binding strength of the indirect layer H_2 (about −0.04 eV) is much weaker than that of the first layer H_2 (about −0.08 eV). The differential charge density isosurface of the maximum concentration $H_{80}C_{96}Li_6$ (Figure 6b) clearly illustrates the polarization of all adsorption H_2 and the difference of the polarized degrees between the two layers. Region I depicts the direct adsorption of H_2, and region II shows the indirect layer adsorption. It is clear that the H_2 molecules in region I are polarized more remarkable than that in region II, which agrees well with the more favorable binding energy of the direct adsorption.

4. CONCLUSION

A HCN structure with well-aligned nanopores is predicted by first-principles calculations via phase transition of carbon nanotube bundles under compressing. The high surface area and tunable nanoporous size make it a potential candidate for hydrogen storage. Via Li decoration, favorable H_2 adsorption energy can be achieved and the enhanced binding energy can be attributed to the interaction between polarized H_2 and positive Li ion. The weight percentage and volumetric density of hydrogen storage can reach 6.28 wt % and 102 g/L, respectively, indicating the HCN structure is promising candidate of hydrogen storage medium.

■ ASSOCIATED CONTENT

Supporting Information

Including details of stability of (24, 0) HCN, the configurations of H_2 adsorbed Li@HCN, the vdW corrections of the H_2 binding energy in Li@HCN, and the ZPE correction. The Supporting Information is available free of charge on the ACS Publications website at DOI: 10.1021/acs.jpcc.5b02312.

■ AUTHOR INFORMATION

Corresponding Authors

*E-mail bshan@mail.hust.edu.cn (B.S.).
*E-mail rongchen@mail.hust.edu.cn (R.C.).

Notes

The authors declare no competing financial interest.

■ ACKNOWLEDGMENTS

This work is supported by National Basic Research Program of China (2013CB934800), National Natural Science Foundation of China (Grants 51302094 and 51101064), the Hubei Province Funds for Distinguished Young Scientists (2014CFA018 and 2015CFA034), Fundamental Research Funds for the Central Universities, HUST(2015QN009 and 2014TS037), the State Key Laboratory of Digital Manufacturing Equipment and Technology Funding (DMET2015A01), as well as the Program for Changjiang Scholars and Innovative Research Team in University(IRT13017), and National Engineering Research Center for Nanomedicine. Rong Chen acknowledges the Thousand Young Talents Plan. The calculations are done at

DOI: 10.1021/acs.jpcc.5b02312
J. Phys. Chem. C 2015, 119, 15831−15838

the Texas Advanced Computing Center (TACC) at The University of Texas at Austin.

REFERENCES

(1) http://www1.eere.energy.gov/hydrogenandfuelcells/storage/.

(2) Ming, W. M.; Fang, Z. Z.; Liu, F. Effects of Li Doping on H-Diffusion in MgH_2: A First-Principles Study. *J. Appl. Phys.* **2013**, *114*, 243502.

(3) Dillon, A. C.; Jones, K. M.; Bekkedahl, T. A.; Kiang, C. H.; Bethune, D. S.; Heben, M. J. Storage of Hydrogen in Single-Walled Carbon Nanotubes. *Nature* **1997**, *386*, 377.

(4) Ding, F.; Lin, Y.; Krasnov, P. O.; Yakobson, B. I. Nanotube Derived Carbon Foam for Hydrogen Storage. *J. Chem. Phys.* **2007**, *127*, 164703.

(5) Lee, S. Y.; Park, S. J. Influence of the Pore Size in Multi-walled Carbon Nanotubes on the Hydrogen Storage Behaviors. *J. Solid State Chem.* **2012**, *194*, 307−312.

(6) Ihm, Y.; Cooper, V. R.; Peng, L.; Morris, J. R. The Influence of Dispersion Interactions on the Hydrogen Adsorption Properties of Expanded Graphite. *J. Phys.: Condens. Matter* **2012**, *24*, 424205.

(7) Kim, B. H.; Hong, W. G.; Moon, H. R.; Lee, S. M.; Kim, J. M.; Kang, S.; Jun, Y.; Kim, H. J. Investigation on the Existence of Optimum Interlayer Distance for H_2 Uptake Using Pillared-graphene Oxide. *Int. J. Hydrogen Energy* **2012**, *37*, 14217−14222.

(8) Georgakis, M.; Stavropoulos, G.; Sakellaropoulos, G. P. Alteration of Graphene Based Slit Pores and the Effect on Hydrogen Molecular Adsorption: A Simulation Study. *Microporous Mesoporous Mater.* **2014**, *191*, 67−73.

(9) An, H.; Liu, C. S.; Zeng, Z. Radial Deformation-induced High-capacity Hydrogen Storage in Li-Coated Zigzag Boron Nanotubes. *Phys. Rev. B* **2011**, *83*, 115456.

(10) Liu, Y.; Brown, C. M.; Neumann, D. A.; Geohegan, D. B.; Puretzky, A. A.; Rouleau, C. M.; Hu, H.; Styers-Barnett, D.; Krasnov, P. O.; Yakobson, B. I. Metal-Assisted Hydrogen Storage on Pt-Decorated Single-Walled Carbon Nanohorns. *Carbon* **2012**, *50*, 4953−4964.

(11) Yildirim, T.; Ciraci, S. Titanium-Decorated Carbon Nanotubes as a Potential High-Capacity Hydrogen Storage Medium. *Phys. Rev. Lett.* **2005**, *94*, 175501.

(12) Chakraborty, B.; Modak, P.; Banerjee, S. Hydrogen Storage in Yttrium-Decorated Single Walled Carbon Nanotube. *J. Phys. Chem. C* **2012**, *116*, 22502−22508.

(13) Cabria, I.; López, M. J.; Fraile, S.; Alonso, J. A. Adsorption and Dissociation of Molecular Hydrogen on Palladium Clusters Supported on Graphene. *J. Phys. Chem. C* **2012**, *116*, 21179−21189.

(14) Nachimuthu, S.; Lai, P. J.; Jiang, J. C. Efficient Hydrogen Storage in Boron Doped Graphene Decorated by Transition Metals − A First-Principles Study. *Carbon* **2014**, *73*, 132−140.

(15) López, M. J.; Cabria, I.; Alonso, J. A. Palladium Clusters Anchored on Graphene Vacancies and Their Effect on the Reversible Adsorption of Hydrogen. *J. Phys. Chem. C* **2014**, *118*, 5081−5090.

(16) Li, C.; Li, J.; Wu, F.; Li, S. S.; Xia, J. B.; Wang, L. W. High Capacity Hydrogen Storage in Ca Decorated Graphyne: A First-Principles Study. *J. Phys. Chem. C* **2011**, *115*, 23221−23225.

(17) Zhang, H.; Zhao, M.; Bu, H.; He, X.; Zhang, M.; Zhao, L.; Luo, Y. Ultra-high Hydrogen Storage Capacity of Li-decorated Graphyne: A First-Principles Prediction. *J. Appl. Phys.* **2012**, *112*, 084305.

(18) Kubas, G. J. Molecular Hydrogen Complexes: Coordination of a.Sigma. Bond to Transition Metals. *Acc. Chem. Res.* **1988**, *21*, 120−128.

(19) Psofogiannakis, G. M.; Steriotis, T. A.; Bourlinos, A. B.; Kouvelos, E. P.; Charalambopoulos, G. C.; Stubos, A. K.; Froudakis, G. E. Enhanced Hydrogen Storage by Spillover on Metal-Doped Carbon Foam: an Experimental and Computational Study. *Nanoscale* **2011**, *3*, 933−936.

(20) Gan, Y. J.; Sun, L. T.; Banhart, F. One- and Two-Dimensional Diffusion of Metal Atoms in Graphene. *Small* **2008**, *4*, 587−591.

(21) Cabria, I.; López, M. J.; Alonso, J. A. Theoretical Study of the Transition from Planar to Three-dimensional Structures of Palladium Clusters Supported on Graphene. *Phys. Rev. B* **2010**, *81*, 035403.

(22) Yoon, M.; Yang, S.; Hicke, C.; Wang, E.; Geohegan, D.; Zhang, Z. Calcium as the Superior Coating Metal in Functionalization of Carbon Fullerenes for High-Capacity Hydrogen Storage. *Phys. Rev. Lett.* **2008**, *100*, 206806.

(23) Ao, Z. M.; Peeters, F. M. High-Capacity Hydrogen Storage in Al-adsorbed Graphene. *Phys. Rev. B* **2010**, *81*, 205406.

(24) Huang, S.; Miao, L.; Xiu, Y. J.; Wen, M.; Li, C.; Zhang, L.; Jiang, J. J. Lithium-decorated Oxidized Porous Graphene for Hydrogen Storage by First Principles Study. *J. Appl. Phys.* **2012**, *112*, 124312.

(25) Gao, Y.; Zhao, N.; Li, J.; Liu, E.; He, C.; Shi, C. Hydrogen Spillover Storage on Ca-decorated Graphene. *Int. J. Hydrogen Energy* **2012**, *37*, 11835.

(26) Cui, S.; Zhao, N.; Shi, C.; Feng, C.; He, C.; Li, J.; Liu, E. Effect of Hydrogen Molecule Dissociation on Hydrogen Storage Capacity of Graphene with Metal Atom Decorated. *J. Phys. Chem. C* **2014**, *118*, 839−844.

(27) Wang, Y.; Li, A.; Wang, K.; Guan, C.; Deng, W.; Li, C.; Wang, X. Reversible Hydrogen Storage of Multi-wall Carbon Nanotubes Doped with Atomically Dispersed Lithium. *J. Mater. Chem.* **2010**, *20*, 6490−6494.

(28) Sigal, A.; Rojas, M. I.; Leiva, E. P. M. Is Hydrogen Storage Possible in Metal-Doped Graphite 2D Systems in Conditions Found on Earth? *Phys. Rev. Lett.* **2011**, *107*, 158701.

(29) Jiang, H. L.; Liu, B.; Lan, Y. Q.; Kuratani, K.; Akita, T.; Shioyama, H.; Zong, F.; Xu, Q. From Metal-Organic Framework to Nanoporous Carbon: Toward a Very High Surface Area and Hydrogen Uptake. *J. Am. Chem. Soc.* **2011**, *133*, 11854−11857.

(30) Gogotsi, Y.; Dash, R. K.; Yushin, G.; Yildirim, T.; Laudisio, G.; Fischer, J. E. Tailoring of Nanoscale Porosity in Carbide-Derived Carbons for Hydrogen Storage. *J. Am. Chem. Soc.* **2005**, *127*, 16006−16007.

(31) Gallego, N. C.; He, L.; Saha, D.; Contescu, C. I.; Melnichenko, Y. B. Hydrogen Confinement in Carbon Nanopores: Extreme Densification at Ambient Temperature. *J. Am. Chem. Soc.* **2011**, *133*, 13794−13797.

(32) Assfour, B.; Seifert, G. Adsorption of Hydrogen in Covalent Organic Frameworks: Comparison of Simulations and Experiments. *Microporous Mesoporous Mater.* **2010**, *133*, 59−65.

(33) Czaja, A. U.; Trukhan, N.; Müller, U. Industrial Applications of Metal−Organic Frameworks. *Chem. Soc. Rev.* **2009**, *38*, 1284−1293.

(34) Dixit, M.; Maark, T. A.; Pal, S. Ab Initio and Periodic DFT Investigation of Hydrogen Storage on Light Metal-Decorated MOF-5. *Int. J. Hydrogen Energy* **2011**, *36*, 10816−10827.

(35) Zou, X.; Zhou, G.; Duan, W.; Choi, K.; Ihm, J. A Chemical Modification Strategy for Hydrogen Storage in Covalent Organic Frameworks. *J. Phys. Chem. C* **2010**, *114*, 13402−13407.

(36) Wu, M. M.; Wang, Q.; Sun, Q.; Jena, P.; Kawazoe, Y. First-Principles Study of Hydrogen Adsorption in Metal-Doped COF-10. *J. Chem. Phys.* **2010**, *133*, 154706.

(37) Langmi, H. W.; Ren, J.; North, B.; Mathe, M.; Bessarabov, D. Hydrogen Storage in Metal-Organic Frameworks: A Review. *Electrochim. Acta* **2014**, *128*, 368−392.

(38) Li, Y. W.; Yang, R. T. Hydrogen Storage in Metal−Organic Frameworks by Bridged Hydrogen Spillover. *J. Am. Chem. Soc.* **2006**, *128*, 8136.

(39) Mendoza-Cortés, J. L.; Han, S. S.; Goddard, W. A. High H_2 Uptake in Li-, Na-, K-Metalated Covalent Organic Frameworks and Metal Organic Frameworks at 298 K. *J. Phys. Chem. A* **2012**, *116*, 1621−1631.

(40) Mendoza-Cortés, J. L.; Goddard, W. A.; Furukawa, H.; Yaghi, O. M. A Covalent Organic Framework that Exceeds the DOE 2015 Volumetric Target for H_2 Uptake at 298 K. *J. Phys. Chem. Lett.* **2012**, *3*, 2671−2675.

(41) Kresse, G.; Joubert, D. From Ultrasoft Pseudopotentials to the Projector Augmented-Wave Method. *Phys. Rev. B* **1999**, *59*, 1758.

(42) Kresse, G.; Hafner, J. Ab Initio Molecular Dynamics for Liquid Metals. *Phys. Rev. B* **1993**, *47*, 558.

(43) Kresse, G.; Hafner, J. Ab Initio Molecular-Dynamics Simulation of the Liquid-Metal-Amorphous-Semiconductor Transition in Germanium. *Phys. Rev. B* **1994**, *49*, 14251.

DOI: 10.1021/acs.jpcc.5b02312
J. Phys. Chem. C 2015, 119, 15831−15838

(44) Kresse, G.; Hafner, J. Efficiency of Ab-initio Total Energy Calculations for Metals and Semiconductors Using a Plane-Wave Basis Set. *Comput. Mater. Sci.* **1996**, *6*, 15−50.
(45) Tada, K.; Furuya, S.; Watanabe, K. Ab Initio Study of Hydrogen Adsorption to Single-Walled Carbon Nanotubes. *Phys. Rev. B* **2001**, *63*, 155405.
(46) Sahaym, U.; Norton, M. G. Advances in the Application of Nanotechnology in Enabling a 'Hydrogen Economy'. *J. Mater. Sci.* **2008**, *43*, 5395−5429.
(47) Cha, J.; Lim, S.; Choi, C. H.; Cha, M.; Park, N. Inaccuracy of Density Functional Theory Calculations for Dihydrogen Binding Energetics onto Ca Cation Centers. *Phys. Rev. Lett.* **2009**, *103*, 216102.
(48) Cabria, I.; López, M. J.; Alonso, J. A. Hydrogen Storage in Pure and Li-doped Carbon Nanopores: Combined Effects of Concavity and Doping. *J. Chem. Phys.* **2008**, *128*, 144704.
(49) Beheshti, E.; Nojeh, A.; Servati, P. A First-principles Study of Calcium-Decorated, Boron-Doped Graphene for High Capacity Hydrogen Storage. *Carbon* **2011**, *49*, 1561−1567.
(50) Liu, W.; Zhao, Y. H.; Li, Y.; Jiang, Q.; Lavernia, E. J. Enhanced Hydrogen Storage on Li-Dispersed Carbon Nanotubes. *J. Phys. Chem. C* **2009**, *113*, 2028−2033.
(51) Cabria, I.; López, M. J.; Alonso, J. A. Enhancement of Hydrogen Physisorption on Graphene and Carbon Nanotubes by Li Doping. *J. Chem. Phys.* **2005**, *123*, 204721.
(52) Grimme, S.; Antony, J.; Ehrlich, S.; Krieg, S. A Consistent and Accurate Ab Initio Parametrization of Density Functional Dispersion Correction (dft-d) for the 94 Elements H-Pu. *J. Chem. Phys.* **2010**, *132*, 154104.
(53) Klimeš, J.; Bowler, D. R.; Michaelides, A. Chemical Accuracy for the Van Der Waals Density Functional. *J. Phys.: Condens. Matter* **2010**, *22*, 022201.
(54) Wen, Y. W.; Liu, H. J.; Pan, L.; Tan, X. J.; Lv, H. Y.; Shi, J.; Tang, X. F. A Triplet Form of (5,0) Carbon Nanotube with Higher Hydrogen Storage Capacity. *J. Phys. Chem. C* **2011**, *115*, 9227−9231.
(55) Wen, Y. W.; Liu, X.; Duan, X.; Cho, K.; Chen, R.; Shan, B. Theoretical Study of sp^2-sp^3 Hybridized Carbon Network for Li-ion Battery Anode. *J. Phys. Chem. C* **2013**, *117*, 4951−4956.
(56) Zang, J.; Treibergs, A.; Han, Y.; Liu, F. Geometric Constant Defining Shape Transitions of Carbon Nanotubes under Pressure. *Phys. Rev. Lett.* **2004**, *92*, 105501.
(57) Cai, J. Z.; Lu, L.; Kong, W. J.; Zhu, H. W.; Zhang, C.; Wei, B. Q.; Wu, D. H.; Liu, F. Pressure-Induced Transition in Magnetoresistance of Single-Walled Carbon Nanotubes. *Phys. Rev. Lett.* **2006**, *97*, 026402.
(58) Henkelman, G.; Arnaldsson, A.; Jonsson, H. A Fast and Robust Algorithm for Bader Decomposition of Charge Density. *Comput. Mater. Sci.* **2006**, *36*, 354−360.
(59) Tang, W.; Sanville, E.; Henkelman, G. A Grid-Based Bader Analysis Algorithm without Lattice Bias. *J. Phys.: Condens. Matter* **2009**, *21*, 084204.
(60) Michael, D.; Mingos, P. A Historical Perspective on Dewar's Landmark Contribution to Organometallic Chemistry. *J. Organomet. Chem.* **2001**, *635*, 1.
(61) Bhatia, S. K.; Myers, A. L. Optimum Conditions for Adsorptive Storage. *Langmuir* **2006**, *22*, 1688−1700.
(62) Yoon, M.; Yang, S.; Wang, E.; Zhang, Z. Charged Fullerenes As High-Capacity Hydrogen Storage Media. *Nano Lett.* **2007**, *7*, 2578.

DOI: 10.1021/acs.jpcc.5b02312
J. Phys. Chem. C 2015, 119, 15831−15838